



# *Atmospheric pressure ultraviolet laser desorption and ionization from liquid samples for native mass spectrometry*

Article

Published Version

Creative Commons: Attribution 4.0 (CC-BY)

Open Access

Hale, O. and Cramer, R. (2019) Atmospheric pressure ultraviolet laser desorption and ionization from liquid samples for native mass spectrometry. *Analytical Chemistry*, 91 (22). pp. 14192-14197. ISSN 0003-2700 doi: <https://doi.org/10.1021/acs.analchem.9b03875> Available at <http://centaur.reading.ac.uk/87024/>

It is advisable to refer to the publisher's version if you intend to cite from the work. See [Guidance on citing](#).

To link to this article DOI: <http://dx.doi.org/10.1021/acs.analchem.9b03875>

Publisher: American Chemical Society

All outputs in CentAUR are protected by Intellectual Property Rights law, including copyright law. Copyright and IPR is retained by the creators or other copyright holders. Terms and conditions for use of this material are defined in

the [End User Agreement](#).

[www.reading.ac.uk/centaur](http://www.reading.ac.uk/centaur)

## **CentAUR**

Central Archive at the University of Reading

Reading's research outputs online

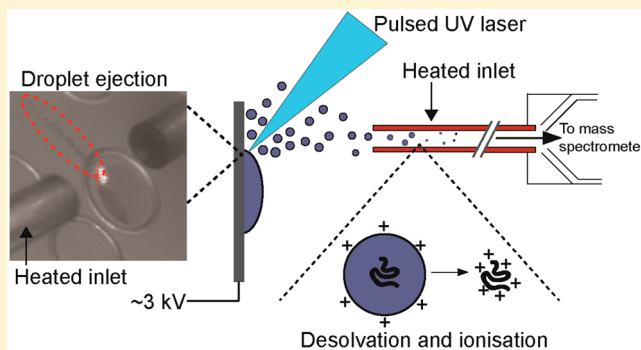
# Atmospheric Pressure Ultraviolet Laser Desorption and Ionization from Liquid Samples for Native Mass Spectrometry

Oliver J. Hale<sup>#</sup> and Rainer Cramer<sup>\*†</sup>

Department of Chemistry, University of Reading, Whiteknights, Reading RG6 6AD, United Kingdom

## Supporting Information

**ABSTRACT:** Understanding protein structure is vital for evaluating protein interactions with drugs, proteins, and other ligands. Native mass spectrometry (MS) is proving to be invaluable for this purpose, enabling analysis of “native-like” samples that mimic physiological conditions. Native MS is usually performed by electrospray ionization (ESI) with its soft ionization processes and the generation of multiply charged ions proving favorable for conformation retention and high mass analysis, respectively. There is scope to expand the currently available toolset, specifically to other soft ionization techniques such as soft laser desorption, for applications in areas like high-throughput screening and MS imaging. In this Letter, observations made from native MS experiments using an ultraviolet (UV) laser-based ion source operating at atmospheric pressure are described. The ion source is capable of producing predominately multiply charged ions similar to ESI. Proteins and protein complexes were analyzed from a native-like sample droplet to investigate the technique. Ion mobility-mass spectrometry (IM-MS) measurements showed that folded protein conformations were detected for ions with low charge states. This observation indicates the source is suitable for native MS analysis and should be further developed for higher mass analysis in the future.



The soft ionization techniques electrospray ionization (ESI) and nanoESI are used extensively for analysis of samples in “native-like” conditions by mass spectrometry (native MS). Samples are analyzed from solutions that mimic a physiological environment.<sup>1</sup> The ion source is operated at atmospheric pressure (AP), where ions in the spray are cooled, and solvent molecules are removed from the analyte ions by gentle collisions with gaseous molecules. Low emitter voltages are used, with narrow-bore (<5 μm internal diameter) emitters aiding sample desalting.<sup>1,2</sup> This limits the internal energy gain and unfolding of protein ions as they are passed from solution into the gas phase and the vacuum of the mass spectrometer. Protein structures, as present under physiological conditions, may be preserved. This is particularly important for ion mobility-mass spectrometry (IM-MS) instruments, which are capable of gas-phase evaluation of the 3-dimensional protein ion structure.<sup>3,4</sup> Values for collisional cross sections (CCSs) may be determined from IM-MS experiments, allowing ion conformations to be compared between systems and techniques.

Other ion sources are being adopted for native MS. Desorption electrospray ionization (DESI) has shown promise, allowing the lifting of complexes from a planar surface by a charged solvent beam and subsequent analysis by MS.<sup>5</sup> Similarly, liquid extraction surface analysis (LESA) has been demonstrated for the analysis of native proteins directly from tissue sections.<sup>6</sup>

Native MS has also been described with laser-based ion sources. Like ESI, matrix-assisted laser desorption/ionization (MALDI) MS has been used to analyze proteins since the late 1980s<sup>7</sup> and to detect noncovalent protein complexes and intact quaternary protein structures.<sup>8</sup> The typical solid-state MALDI samples predominantly produce singly charged ions and are thus usually analyzed using high mass range TOF analyzers. However, multiply charged ions may be produced using an AP ion source and liquid samples.<sup>9</sup> In the case of ultraviolet (UV)-MALDI, the use of typically acidic liquid support matrices (LSMs) produces highly charged ions in the positive ion mode, while basic LSMs are beneficial for producing highly charged ions in the negative ion mode.<sup>10</sup> Proteins as large as apo-transferrin (approximately 80 kDa) have been analyzed in this way.<sup>11</sup> However, these sample conditions are not suitable for native MS. Beaufour et al. were able to demonstrate native-like analysis using a high vacuum MALDI source with an ionic liquid matrix made up of an organic acid, organic base, and glycerol.<sup>12</sup> The protein ions formed were largely singly charged, as expected of the instrumentation used, in the  $m/z$  range of 9000–20 000. This is beyond the optimal  $m/z$  range of many commercial high-performance mass spectrometers, such as QTOF and hybrid Orbitrap instruments (although the

Received: August 23, 2019

Accepted: October 25, 2019

Published: October 25, 2019

options for high  $m/z$  analysis have improved over the past decade), and thus, the available MS/MS techniques, mass resolution, and accuracy as well as access to IM-MS are limited.

A mixture of native and denatured states was observed by Lu et al. with the desorption by impulsive vibrational excitation (DIVE-MS) setup.<sup>13</sup> The employed system used a picosecond infrared laser (PIRL) to ablate material from a liquid sample. Native-like protein analysis was demonstrated but did not feature ion mobility measurements. Other studies have made use of lasers for sample vaporization but relied on ESI post-ionization. These laser ablation electrospray ionization (LAESI) systems have been shown to preserve the protein native state and have higher tolerance to salts than ESI alone.<sup>14,15</sup>

In this Letter, we demonstrate native MS analysis of the monomeric protein hen egg white lysozyme (HEWL) and other proteins using a simple AP-MALDI ion source with a low-cost UV laser, generating multiply charged MALDI protein ions on a commercial high-performance QTOF instrument with ion mobility separation. A material ejection phenomenon resulting from the interaction of the laser with the sample plate was exploited to allow the vaporization of liquid samples not usually compatible with UV MALDI analysis.

## MATERIALS AND METHODS

Bovine ubiquitin, horse heart myoglobin, hen egg white lysozyme (HEWL), jack-bean concanavilin A (ConA), 2,5-dihydroxybenzoic acid (DHB), ammonium acetate, and ethylene glycol were bought from Sigma-Aldrich (Gillingham, UK). HPLC grade water and acetonitrile were bought from Fisher Scientific (Loughborough, UK). Sodium iodide solution (2  $\mu\text{g}/\mu\text{L}$ ) was obtained from Waters (Manchester, UK). Nitrogen, argon, and helium gases (all >99.99% pure) were obtained from Air Liquide UK Ltd. (Stoke-on-Trent, UK).

The neutral liquid MALDI matrix (neutral matrix) consisted of ethylene glycol dissolved in an aqueous ammonium acetate solution (200 mM) in a ratio of 3:5 (v/v), resulting in a pH value of approximately 7. The acidic liquid MALDI matrix (acidic matrix) was DHB dissolved at a concentration of 25 mg/mL in water/acetonitrile/ethylene glycol (3:7:6; v/v/v) with a pH value of approximately 2, which has previously been demonstrated to produce highly protonated protein ions.<sup>10,11</sup> Sodium iodide solution was used as provided for calibration of the TOF analyzer in the  $m/z$  range of 100–8000 by AP-LDI. A volume of 500 nL of the sodium iodide solution was spotted with 500 nL of ethylene glycol/water (3:5; v/v) and analyzed by ablating material from the droplet edge. For calibration of the TWIMS cell, ubiquitin and myoglobin were dissolved to 200 pmol/ $\mu\text{L}$  in 0.1% formic acid. A volume of 500 nL of protein solution was spotted on the MALDI target plate with 500 nL of the acidic matrix solution to give an in-droplet amount of 100 pmol of protein. The actual sample volume was less than 1  $\mu\text{L}$  due to some evaporation of solvents. Proteins were dissolved to 200 pmol/ $\mu\text{L}$ , except ConA which was dissolved to 10 pmol/ $\mu\text{L}$ , in an aqueous ammonium acetate solution (200 mM) and spotted in equal volumes with the neutral matrix to give an in-droplet amount of 100 pmol (5 pmol for ConA) for native-like analysis.

A custom AP-MALDI ion source was attached to a Synapt G2-Si (Waters) as detailed previously.<sup>16</sup> Briefly, a pulsed UV laser (337 nm, 1–30 Hz repetition rate, 3 ns pulse duration, approximately 20  $\mu\text{J}$  per pulse) was mounted atop the mass spectrometer, and the beam was directed through a lens with a

focal length of 150 mm onto the stainless-steel MALDI target plate. A potential of 3 kV was applied to the MALDI target plate with approximately 5 mm between the target plate surface and the instrument's inlet. The inlet ion transfer tube was operated at approximately 100 °C without counter-flow gas. The ion block temperature was set to 80 °C, and the cone voltage was set to 30–40 V for best analyte ion signal intensity. The mass spectrometer was operated in “positive ion mode”, “ion mobility-TOF”, and “sensitivity” mode. The backing pressure was approximately 2.6 mbar. Data were collected over the  $m/z$  range of 100–5000 with an automatic quadrupole profile and TOF scan duration of 1 s. The collision cell gas was argon, providing a pressure of approximately  $2.3 \times 10^{-2}$  mBar in the trap and transfer cells, raised to  $3.2 \times 10^{-2}$  mBar for native myoglobin and ConA analysis. Helium was provided to the helium cell to give a pressure of approximately 3.8 mbar. The TWIMS drift gas was nitrogen, resulting in a pressure of approximately 2.6 mbar in the TWIMS device. The normalized collision potential applied in the trap cell was 4 V and in the transfer cell was 30 V. The IM wave velocity was 650 m/s with a wave height of 40 V. The trap DC bias was set between 40 and 45 V. Settings were unchanged between the calibration and analysis steps, and the instrument was kept in the “Operate” state between analyses to maintain stable pressures, temperatures, and voltages. Laboratory temperature was approximately 20 °C. Full IM-MS parameters as recorded by the instrument can be found in the “\_extern.inf” file included with each raw datafile. These are available in the University of Reading's Research Data Archive.

Calibration of the TWIMS cell was performed by liquid AP-MALDI IM-MS analysis (IM settings as described above) of ubiquitin and apo-myoglobin using the acidic matrix, with reference to published protocols and  $^{DT}CCS_{N_2}$  values of denatured proteins analyzed by ESI drift tube ion mobility-MS.<sup>4,17</sup> Calculations were performed using the CCS calculation spreadsheet by Hofmann and Pagel ([https://www.bcp.fu-berlin.de/en/chemie/chemie/forschung/OrgChem/pagel/resources/research/CCS\\_calibration\\_spreadsheet\\_2014.xlsx](https://www.bcp.fu-berlin.de/en/chemie/chemie/forschung/OrgChem/pagel/resources/research/CCS_calibration_spreadsheet_2014.xlsx)). The arrival time (in ms), obtained from the apex of the most intense mobility peak, was determined for each charge state using Driftscope 2.8 and MassLynx 4.1 (Waters). Corrected drift time ( $dt'$ ) was calculated with eq 1:

$$dt' = dt - \left[ \frac{C\sqrt{m/z}}{1000} \right] \quad (1)$$

where  $C$  is the enhanced duty cycle (EDC) delay coefficient (1.41 ms) and  $dt$  is the measured arrival time. Corrected CCS ( $CCS'$ ) was calculated with eq 2:

$$CCS' = \frac{CCS}{\left[ z \left( \frac{1}{\mu} \right)^{1/2} \right]} \quad (2)$$

where  $CCS$  is the calibrant literature CCS value,  $\mu$  is the ions' reduced mass, and  $z$  is the ion charge state. A logarithmic fit was applied to a plot of  $\ln(CC'S')$  vs  $\ln(dt')$ , with a coefficient of determination  $R^2 = 0.9955$ . New corrected drift times ( $dt''$ ) were obtained by eq 3:

$$dt'' = dt'^{\alpha} \times z \times \left( \frac{1}{\mu} \right)^{1/2} \quad (3)$$

where  $x$  is the slope of the log plot.  $^{TW}CCS_{N_2}$  ( $CCS$  obtained using a traveling wave device under  $N_2$ ) were then calculated as the product of  $dt''$  and the log plot constant ( $A$ ).  $CCS_{N_2}$  values were also calculated by the trajectory method (TM) in IMoS 1.09 from crystal structure data.<sup>18</sup> Where applicable, spectrum deconvolution was performed with UniDec (version 3.2.0; Oxford, UK).<sup>19</sup> Collision-induced unfolding plots in the Supporting Information were produced with ORIGAMI (version 1.2.1.4; Manchester, UK).<sup>20</sup>

## RESULTS AND DISCUSSION

It is first important to note that, for the analyses performed with the acidic matrix, the laser could be focused at any point on the droplet to detect analyte ion signal. However, the best total ion count was usually achieved from the center of the droplet. When analyzing a sample not containing a UV-MALDI chromophore, it was necessary to focus the laser on the droplet edge in order to cause effective ablation. Figure S1 shows a photograph of a stream of ablated droplets across the MALDI target plate surface, often seen when analyzing a neutral pH sample in this way.

Ubiquitin was analyzed with the acidic and neutral matrices. The acidic matrix resulted in highly charged ions with a wide charge state distribution (CSD) suitable for calibration of the TWIMS data (Figure S2a). The neutral matrix predominantly resulted in  $5^+$  and  $6^+$  analyte ions (Figure S2b). Investigation of the ion arrival time distributions (ATDs) for the  $4^+$ ,  $5^+$ , and  $6^+$  charge states (Figure S2c–e, respectively) revealed multiple conformations. Some more folded conformations were detected as revealed by  $^{TW}CCS_{N_2}$  for each ATD peak and comparison to previously reported values.<sup>21</sup>

Figure 1a shows a typical liquid AP-MALDI mass spectrum for HEWL when analyzed with the acidic matrix, while Figure 1b shows a spectrum produced with the neutral matrix. In general, the most intense charge state observed was  $[M + 11H]^{11+}$  for the acidic matrix, but  $[M + 8H]^{8+}$  for the “native-like” neutral pH sample where lower charge states were favored.

Interestingly, the most intense ion signal, besides  $[M + nH]^{n+}$ , for the “native-like” sample is  $[M + Fe(II) + (n - 2)H]^{n+}$ . Iron is most likely derived from the stainless-steel MALDI target plate. The observed adduct ions are probably formed within the laser-ablated liquid microdroplets as they are desolvated. Iron may coordinate with, and reversibly inactivate, lysozyme in solution.<sup>22,23</sup> No measurable difference in  $^{TW}CCS_{N_2}$  was observed for iron adduct ions compared to protonated ions, suggesting that iron coordination does not result in HEWL unfolding. The approximate mass difference between  $[M + nH]^{n+}$  and  $[M + Fe + (n - 2)H]^{n+}$  ions is 54 Da (see Figure S3), indicating a two-proton difference compared to the protonated molecular ion, thus suggesting the iron coordinated in the 2+ oxidation state. Interestingly, this contrasts with previous research where Fe(III) was detected bound to HEWL by ESI MS, perhaps indicating that the iron ions are located differently on HEWL ions produced in the gas phase than when allowed to interact with HEWL in solution prior to ionization.<sup>23</sup> Sodium and potassium adduct ions were also observed. In contrast, the most abundant adduct ion when analyzed with the acidic matrix is  $[M + nH + DHB]^{n+}$ , whereas the iron adducts were absent. This is likely because direct laser ablation of the target plate surface is virtually prohibited by the strong absorption of the acidic matrix chromophore and small laser penetration depth.

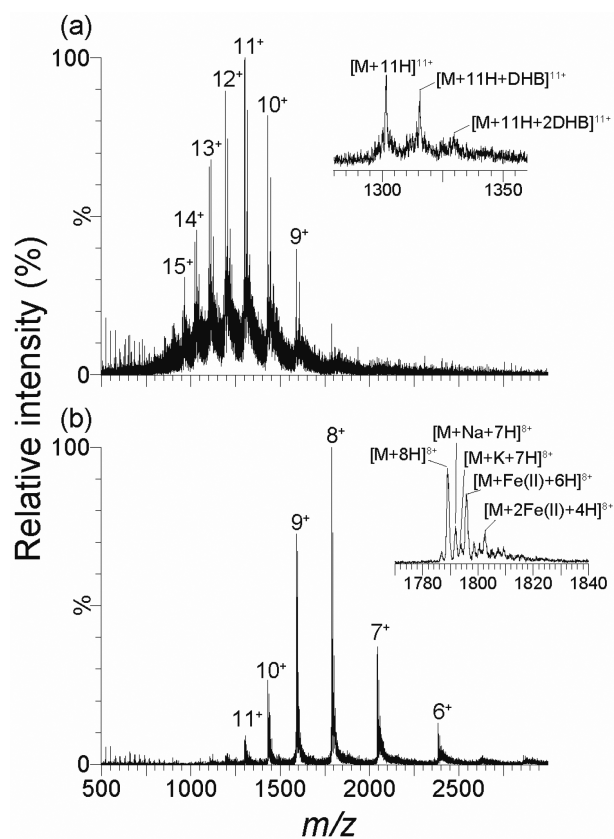


**Figure 1.** AP-(MA)LDI mass spectra for HEWL (100 pmol per droplet) from liquid samples. (a) Charge states up to  $15^+$  were detected for a sample prepared with a DHB/ethylene glycol-based liquid matrix (approximately pH 2). The inset spectrum shows the adduct ions detected for the  $11^+$  charge state. (b) A “native-like” sample using a matrix with 200 mM ammonium acetate and no UV MALDI chromophore (approximately pH 7) resulted in lower charge states being detected. The inset spectrum shows the adduct ions detected for the  $8^+$  charge state.

Unlike for the ubiquitin spectrum, the AP-LDI native mass spectrum in Figure 1b features more charge states than that of HEWL produced by nanoESI, indicating the need for optimization of gentler ionization conditions in the future. In ESI MS, higher charge states are indicative of in-solution unfolding of the protein and ionization by the charge ejection model.<sup>24</sup> However, IM-MS measurements were used in this study to collect further evidence to confirm the preservation of folded conformations when detected by liquid AP-MALDI MS.

For each charge state of HEWL, for which the MS data are shown in Figure 1b, extracted ion ATD plots are presented in Figure 2. The charge states  $11^+$  to  $9^+$  (Figure 2a–c) show peaks indicating unfolded structures, since the  $^{TW}CCS_{N_2}$  values are considerably larger than  $1799 \text{ \AA}^2$  as calculated by the TM from the HEWL crystal structure (Protein Data Bank entry 1DPX).<sup>25</sup> The ATD plot for the  $8^+$  ion (the most intense MS ion signal in Figure 1b) features two peaks (see Figure 2d), indicating two resolvable protein structures. The  $^{TW}CCS_{N_2}$  values of these two peaks ( $1798$  and  $2193 \text{ \AA}^2$ ) suggest one folded and one unfolded conformation, with the former value being very similar to the predicted value. The effect of raising the collision potential in the trap cell can be observed in Figure S4, where the presumably folded conformation is absent above 20 V. The additional energy added to the protein ions prior to

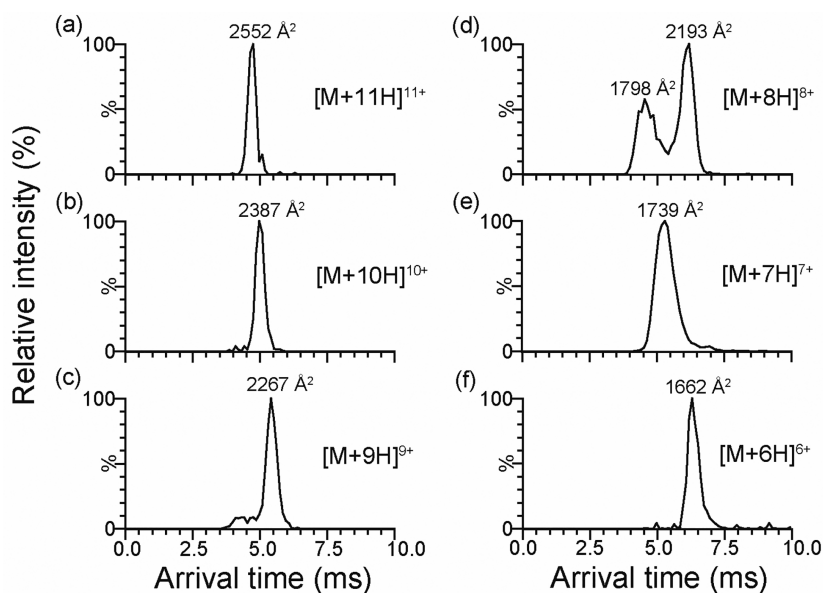


**Figure 2.** Ion arrival time distribution (ATD) plots obtained from the “native-like” HEWL sample for charge states 11<sup>+</sup> to 6<sup>+</sup> (a–f), with <sup>TW</sup>CCS<sub>N2</sub> noted for each peak maximum. Each plot was generated from an approximately ±1.5 Da window around the [M + nH]<sup>n+</sup> peak. The charge states 11<sup>+</sup> to 9<sup>+</sup> (a–c) indicate unfolded structures, whereas 7<sup>+</sup> and 6<sup>+</sup> (e, f) are indicative of folded structures, evidenced by substantially smaller <sup>TW</sup>CCS<sub>N2</sub>. The ATD plot of the 8<sup>+</sup> charge state (d) displays ion populations of both conformations.

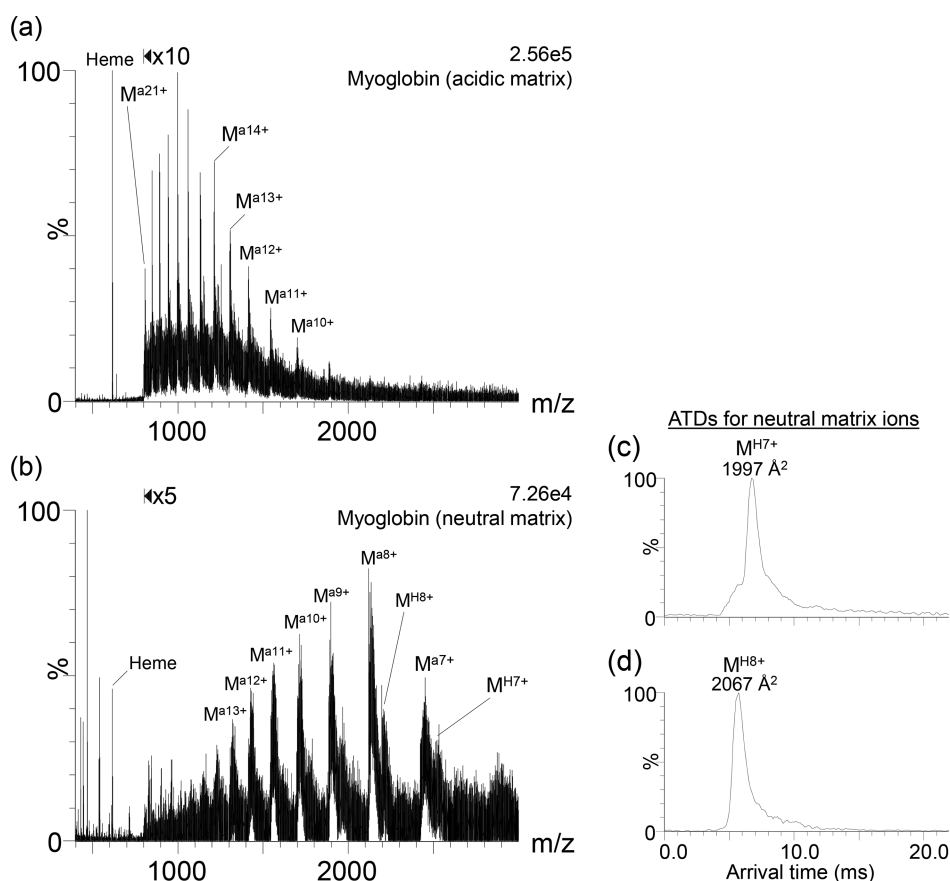


**Figure 3.** AP-(MA)LDI mass spectra for myoglobin obtained from liquid samples using the acidic matrix (a) and neutral matrix (b). Substantially different CSDs were observed. The apo-form of myoglobin (M<sup>a</sup>) was readily detected for both matrices, whereas the heme-binding holo-form (M<sup>H</sup>) was only detected with the neutral matrix at lower charge states. The relative abundance of heme is also lower for the analysis under “native-like” conditions. The <sup>TW</sup>CCS<sub>N2</sub> for the 7<sup>+</sup> (c) and 8<sup>+</sup> (d) holo-form ions correspond closely to previously reported values.<sup>21</sup>

IM separation appear to have caused the folded ions to unfold. The lowest charge states, 7<sup>+</sup> (1739 Å<sup>2</sup>) and 6<sup>+</sup> (1662 Å<sup>2</sup>)

(Figure 2e,f), exhibit smaller <sup>TW</sup>CCS<sub>N2</sub> values than predicted. This again suggests the conformation detected for each is

folded. The 7<sup>+</sup> conformation also experienced unfolding at elevated trap collision potentials (Figure S5). Differences of around 10% in measured CCS values compared to CCS values predicted from crystal structure coordinates are well documented for native MS of monomeric proteins.<sup>26</sup>

To investigate whether noncovalent interactions could be retained, myoglobin was analyzed with the acidic and neutral matrices. High-charge state ions were observed for apo-myoglobin when analyzed using the acidic matrix (Figure 3a), whereas lower charge state ions were produced with the neutral matrix (Figure 3b). Peaks for holo-myoglobin, where the heme is bound noncovalently, were only detected from the neutral matrix alongside apo-myoglobin peaks (Figure S6, mass difference of ~616 Da). The holo-form is an indicator for gentle analysis conditions and the preservation of noncovalent binding in the gas phase. The <sup>TW</sup>CCS<sub>N<sub>2</sub></sub> for holo-myoglobin ions (7<sup>+</sup>, 8<sup>+</sup>) were similar to previously reported values, suggesting the complex was detected in a folded conformation.<sup>21</sup>

Additionally, ConA in ammonium acetate was analyzed using the neutral matrix. By nESI MS, ConA is typically detected as monomer (approximately 25.1 kDa), homodimer (approximately 51.5 kDa), and homotetramer (approximately 103 kDa) at pH 7. Here, we detected homodimers with a narrow CSD (13<sup>+</sup>–16<sup>+</sup>), indicative of native conformations, and monomers with a broader CSD (Figure S7a). The <sup>TW</sup>CCS<sub>N<sub>2</sub></sub> values for the dimer ions (14<sup>+</sup>: 4313 Å<sup>2</sup>; 15<sup>+</sup>: 4300 Å<sup>2</sup>; 16<sup>+</sup>: 4351 Å<sup>2</sup>; Figure S7b) were comparable to CCS<sub>N<sub>2</sub></sub> values predicted from the dimer crystal structure, using the Protein Data Bank entry 1GKB (4412 Å<sup>2</sup>).<sup>27</sup> The 16<sup>+</sup> ions also displayed a second conformer (5099 Å<sup>2</sup>) indicative of some unfolding. The monomer CSD suggests that some degree of thermalization may occur during ionization, producing a mixture of folded and unfolded states. The tetramer was not detectable from the MS data alone. However, the inspection of the 2D ATD plot (Figure S8) revealed a trace that is potentially attributable to tetramer ions. The lack of peak resolution is likely due to the currently lower sensitivity of the AP-LDI method compared to nESI as well as a need to improve ion transmission and desolvation conditions. Previously, the analysis of larger proteins (e.g., apo-transferrin, approximately 78 kDa) has proven challenging even with the efficient acidic matrices.<sup>11</sup> Raising the backing pressure of the mass spectrometer may help to improve large ion focusing and desolvation as is now commonplace for native nESI MS.

The ejection of material by UV laser irradiation from a nonabsorptive liquid droplet is a phenomenon that we have previously utilized to successfully ionize sodium iodide, for calibration purposes, on the AP-MALDI ion source.<sup>10</sup> Koch et al. have suggested that the substrate, in this case the stainless-steel MALDI target plate, supports front sample surface spallation due to rapid heating of the substrate by the incident laser pulse, resulting in the ejection of MALDI sample material.<sup>28</sup> A detailed discussion of the differences of the various ion sources and their effects on ionization is beyond the scope of this Letter, but one common feature is worth noting: the instrument's inlet. In this AP-MALDI study, sample material ejected by the spallation event is captured by the heated MS inlet. It is proposed that the protein ions detected were essentially the product of "ESI-like" processes, collisions with gas molecules and the inlet, and the elevated temperature of the inlet's ion transfer tube, resulting in the release of ions into the gas phase.

In a recent article by Towers et al., it was shown that a heated inlet was essential for promoting protein ion formation by DESI.<sup>29</sup> The DIVE-MS setup also incorporates a heated inlet for analyzing denatured and native protein samples.<sup>13</sup> Comparisons can also be made to solvent-assisted ionization (SAI), where protein-containing solutions are directly introduced to the heated inlet.<sup>30</sup> The inlet temperature for SAI is typically higher than what was used for the AP-MALDI experiments here, presumably necessary due to higher volumes of solvent introduced. It is reasonable to suggest that the laser in the AP-MALDI ion source used here plays a fundamentally limited role in the ionization itself (without a MALDI chromophore included) but is practically an extremely convenient and highly controllable method of introducing small, nebulized volumes of liquid sample to the heated inlet.

## CONCLUSION

This initial report of native-like sample analysis with a UV-AP-MALDI ion source presents an alternative to the usual ESI MS methodologies used for native MS. It offers the ability to analyze low sample volumes and does not require substantial modification to native MS sample preparation. Liquid MALDI has also been shown to be more flexible and tolerant toward contaminants and changes in the sample environment, potentially further widening the range of comparative analyses of various possible protein conformations that depend on the (sample) environment.<sup>31,32</sup> AP-MALDI ion sources are appropriate for high-throughput analysis, for applications such as screening. This ion source requires further development for the analysis of much larger proteins and complexes, as shown by the lack of signal for the ConA tetramer. MALDI is also an established MS imaging technique, and a modified AP-LDI setup could be further investigated as a laser-based native MS imaging platform. Additional modifications could include the addition of a picosecond infrared laser to ablate the sample droplet easily, since water would act as a chromophore, and with limited heating of the sample. This might lead to sensitivity gains, easy high-throughput analysis, and the analysis of much larger analytes.

## ASSOCIATED CONTENT

### Supporting Information

The Supporting Information is available free of charge on the ACS Publications website at DOI: 10.1021/acs.analchem.9b03875.

Image of the laser ablation and droplet ejection; ubiquitin AP-(MA)LDI mass spectra and ATDs; deconvoluted HEWL zero-charge mass spectrum; ATD plots; liquid AP-LDI MS; arrival time–*m/z* plot (PDF)

## AUTHOR INFORMATION

### Corresponding Author

\*E-mail: r.k.cramer@reading.ac.uk.

### ORCID

Rainer Cramer: 0000-0002-8037-2511

### Present Address

#O.J.H.: School of Biosciences, University of Birmingham, Edgbaston, Birmingham, B15 2TT, UK.

### Author Contributions

O.J.H. performed the experimental work. The manuscript was written by O.J.H. and R.C.

## Notes

The authors declare no competing financial interest.

Data supporting the results reported in this paper are openly available from the University of Reading Research Data Archive at <http://dx.doi.org/10.17864/1947.215>.

## ACKNOWLEDGMENTS

This research was supported by the Engineering and Physical Sciences Research Council (EPSRC) (DTG Grant No. 1498422) and Waters Corporation.

## REFERENCES

- (1) Leney, A. C.; Heck, A. J. *J. Am. Soc. Mass Spectrom.* **2017**, *28*, 5–13.
- (2) Nguyen, G. T. H.; Tran, T. N.; Podgorski, M. N.; Bell, S. G.; Supuran, C. T.; Donald, W. A. *ACS Cent. Sci.* **2019**, *5*, 308–318.
- (3) Poltash, M. L.; McCabe, J. W.; Shirzadeh, M.; Laganowsky, A.; Clowers, B. H.; Russell, D. H. *Anal. Chem.* **2018**, *90*, 10472–10478.
- (4) Ruotolo, B. T.; Benesch, J. L. P.; Sandercock, A. M.; Hyung, S.-J.; Robinson, C. V. *Nat. Protoc.* **2008**, *3*, 1139.
- (5) Ambrose, S.; Housden, N. G.; Gupta, K.; Fan, J.; White, P.; Yen, H. Y.; Marcoux, J.; Kleanthous, C.; Hopper, J. T. S.; Robinson, C. V. *Angew. Chem., Int. Ed.* **2017**, *56*, 14463–14468.
- (6) Griffiths, R. L.; Sisley, E. K.; Lopez-Clavijo, A. F.; Simmonds, A. L.; Styles, I. B.; Cooper, H. J. *Int. J. Mass Spectrom.* **2019**, *437*, 23–29.
- (7) Karas, M.; Hillenkamp, F. *Anal. Chem.* **1988**, *60*, 2299–2301.
- (8) Rosinke, B.; Strupat, K.; Hillenkamp, F.; Rosenbusch, J.; Dencher, N.; Krüger, U.; Galla, H.-J. *J. Mass Spectrom.* **1995**, *30*, 1462–1468.
- (9) Cramer, R.; Pirkl, A.; Hillenkamp, F.; Dreisewerd, K. *Angew. Chem., Int. Ed.* **2013**, *52*, 2364–2367.
- (10) Hale, O. J.; Ryumin, P.; Brown, J. M.; Morris, M.; Cramer, R. *Rapid Commun. Mass Spectrom.* **2018**, 1–8.
- (11) Ryumin, P.; Cramer, R. *Anal. Chim. Acta* **2018**, *1013*, 43–53.
- (12) Beaufour, M.; Ginguene, D.; Le Meur, R.; Castaing, B.; Cadene, M. *J. Am. Soc. Mass Spectrom.* **2018**, *29*, 1981.
- (13) Lu, Y.; Pieterse, C. L.; Robertson, W. D.; Miller, R. J. D. *Anal. Chem.* **2018**, *90*, 4422–4428.
- (14) Karki, S.; Shi, F.; Archer, J. J.; Sistani, H.; Levis, R. J. *J. Am. Soc. Mass Spectrom.* **2018**, *29*, 1002–1011.
- (15) Shiea, J.; Yuan, C.-H.; Huang, M.-Z.; Cheng, S.-C.; Ma, Y.-L.; Tseng, W.-L.; Chang, H.-C.; Hung, W.-C. *Anal. Chem.* **2008**, *80*, 4845–4852.
- (16) Ryumin, P.; Brown, J.; Morris, M.; Cramer, R. *Methods* **2016**, *104*, 11–20.
- (17) Bush, M. F.; Hall, Z.; Giles, K.; Hoyes, J.; Robinson, C. V.; Ruotolo, B. T. *Anal. Chem.* **2010**, *82*, 9557–9565.
- (18) Larriba-Andaluz, C.; Hogan, C. J. *J. Chem. Phys.* **2014**, *141*, 194107.
- (19) Marty, M. T.; Baldwin, A. J.; Marklund, E. G.; Hochberg, G. K. A.; Benesch, J. L. P.; Robinson, C. V. *Anal. Chem.* **2015**, *87*, 4370–4376.
- (20) Migas, L. G.; France, A. P.; Bellina, B.; Barran, P. E. *Int. J. Mass Spectrom.* **2018**, *427*, 20–28.
- (21) May, J. C.; Jurnecko, E.; Stow, S. M.; Kratochvil, I.; Kalkhof, S.; McLean, J. A. *Int. J. Mass Spectrom.* **2018**, *427*, 79–90.
- (22) Sellak, H.; Franzini, E.; Hakim, J.; Pasquier, C. *Arch. Biochem. Biophys.* **1992**, *299*, 172–178.
- (23) Croguennec, T.; Nau, F.; Molle, D.; Le Graet, Y.; Brule, G. *Food Chem.* **2000**, *68*, 29–35.
- (24) Konermann, L.; Ahadi, E.; Rodriguez, A. D.; Vahidi, S. *Anal. Chem.* **2013**, *85*, 2–9.
- (25) Weiss, M. S.; Palm, G. J.; Hilgenfeld, R. *Acta Crystallogr., Sect. D: Biol. Crystallogr.* **2000**, *56*, 952–958.
- (26) Jurnecko, E.; Barran, P. E. *Analyst* **2011**, *136*, 20–28.
- (27) Kantardjieff, K. A.; Höchtl, P.; Segelke, B. W.; Tao, F. M.; Rupp, B. *Acta Crystallogr., Sect. D: Biol. Crystallogr.* **2002**, *58*, 735–743.
- (28) Koch, A.; Schnapp, A.; Soltwisch, J.; Dreisewerd, K. *Int. J. Mass Spectrom.* **2017**, *416*, 61–70.
- (29) Towers, M. W.; Karancsi, T.; Jones, E. A.; Pringle, S. D.; Claude, E. *J. Am. Soc. Mass Spectrom.* **2018**, *29*, 2456–2466.
- (30) Wang, B.; Trimpin, S. *Anal. Chem.* **2014**, *86*, 1000–1006.
- (31) Towers, M.; Cramer, R. *Spectroscopy* **2007**, *22*, 29.
- (32) Ryumin, P.; Brown, J.; Morris, M.; Cramer, R. *Int. J. Mass Spectrom.* **2017**, *416*, 20–28.